J Therm Anal Calorim (2010) 101:865–872
DOI 10.1007/s10973-009-0570-x

Formation of gold nanoparticles in diblock copolymer micelles with various reducing agents

Kinetic and thermodynamic studies

S. Papp · L. Kőrösi · B. Gool · T. Dederichs · P. Mela · M. Möller · I. Dékány

Received: 5 August 2009 / Accepted: 13 October 2009 / Published online: 25 November 2009

Abstract Gold nanoparticles (Au NPs) were prepared by the reduction of $HAuCl_4$ acid incorporated into the polar core of poly(styrene)-*block*-poly(2-vinylpyridine) (PS-*b*-P2VP) copolymer micelles dissolved in toluene. The formation of Au NPs was controlled using three reducing agents with different strengths: hydrazine (HA), triethylsilane (TES), and potassium triethylborohydride (PTB). The formation of Au NPs was followed by transmission electron microscopy, UV–Vis spectroscopy, isothermal titration calorimetry (ITC), and dynamic light scattering (DLS). It was found that the strength of the reducing agent determined both the size and the rate of formation of the Au NPs. The average diameters of the Au NPs prepared by reduction with HA, TES, and PTB were 1.7, 2.6, and 8 nm, respectively. The reduction of Au(III) was rapid with HA and PTB. TES proved to be a mild reducing agent for the synthesis of Au NPs. DLS measurements demonstrated swelling of the PS-*b*-P2VP micelles due to the incorporation of $HAuCl_4$ and the reducing agents. The original micellar structure rearranged during the reduction with PTB. ITC measurements revealed that some chemical reactions besides Au NPs formation also occurred in the course of the reduction process. The enthalpy of formation of Au NPs in PS-*b*-P2VP micelles reduced by HA was determined.

Keywords Gold nanoparticles · Heat of nucleation · Diblock copolymer · Micellar solution · Microcalorimetry

S. Papp · L. Kőrösi · I. Dékány (✉)
Supramolecular and Nanostructured Materials Research Group of the Hungarian Academy of Sciences, University of Szeged, Dóm tér 8, 6720 Szeged, Hungary
e-mail: i.dekany@chem.u-szeged.hu

B. Gool · T. Dederichs · P. Mela · M. Möller
Deutsches Wollforschungsinstitut (DWI) an der RWTH-Aachen, Pauwelsstraße 8, 52056 Aachen, Germany

I. Dékány
Department of Physical Chemistry and Material Sciences, University of Szeged, Aradi vértanúk tere 1, 6720 Szeged, Hungary

Introduction

In consequence of their numerous applications (as catalysis or biosensors and in many fields of nanotechnology), gold nanoparticles (Au NPs) have attracted considerable attention and interest [1–3]. The best-known method for Au NP synthesis is the Turkevich reduction method, published in 1951 [4]. The number of publications on the synthesis of Au NPs has grown steadily ever since [4–7]. Various procedures yield Au NPs with specific sizes and geometries. In order to be able to control the Au NPs size and geometry, it is necessary to be acquainted with the mechanism of Au NPs formation, which is, therefore, studied by an ever increasing number of research groups [8–12]. Au NPs formation can be monitored by different experimental methods. Since Au NPs have a characteristic absorption maximum in the visible wavelength range, the simplest method for monitoring their formation is UV–Vis spectroscopy. Changes in the size, geometry, size distribution, and concentration of Au NPs can be determined from the position and intensity of the absorption maximum. Information is thereby obtained on the nucleation, growth, and aggregation processes, and an Au NPs formation mechanism can be formulated [13]. The Mie theory and its developed versions even allow calculation of Au NPs [14]. Sato et al. synthetized Au NPs in aqueous medium, using Surfynol 465 as stabilizer and reducing agent. They

confirmed the formation of a colourless Au(I)–Surfynol complex in the induction period preceding the appearance of Au NPs and established that the reaction is slower in the micellar than in the monomeric system [15]. Yang et al. generated Au NPs by UV irradiation and studied the effects of pH on their growth. They showed that different photochemical processes take place at different pH values and, as a consequence, the kinetics of Au(III) nucleation and growth also vary [16]. We earlier studied the homogeneous and heterogeneous nucleation of Ag and Pd NPs in aqueous medium [17, 18]. We found that the slow continuous nucleation of Ag NPs was followed by a rapid autocatalytic growth phase. The rate of reduction was decelerated by stabilizing polymers in each case, whereas reduction was accelerated by increasing precursor ion concentration.

Structural rearrangements taking place during NPs synthesis can be studied well through in situ dynamic light scattering (DLS) measurements. With this method, aggregation processes can be evaluated on the basis of the collective size of the NPs and the stabilizer molecules surrounding them [19–21]. NPs can be visualized by electron microscopy and various scanning probe microscopic techniques; the disadvantage of these methods, however, is that they can be applied only to NPs films. Relatively slow reduction processes and aggregation can be visualized by periodic freezing of the process and film preparation [17].

Isothermal titration microcalorimetry was first used to track the formation of NPs by Liveri and co-workers in the early 1990s. They synthetized Au and Pd NPs in a water/AOT/*n*-heptane microemulsion [22, 23]. They established that the duration of nucleation is a few nanoseconds, whereas NP growth spans a time period of minutes. Their results showed that the formation (i.e., reduction of precursor ions) is an exothermic process ($\Delta H_f \sim -250$ to -500 kJ mol^{-1}); the extent of exothermicity increases with the NP size. Patakfalvi and Dékány [24] studied the nucleation and growth of Ag NPs in aqueous medium with sodium citrate as stabilizer and hydroquinone as reducing agent. They established that the heat effect detected is basically determined by the ratio of Ag^+ to hydroquinone. They divided the NP formation into three phases: an initial nucleation phase, which is essentially exothermic; an endothermic growth phase; and a subsequent exothermic aggregation process. Kanemaru et al. synthetized bimetal particles by titrating PVP-stabilized Ag NPs with Rh, Pd, and Pt NPs that were also stabilized by PVP, and vice versa. The strong exothermic interparticle interaction led to the spontaneous development of a pseudo-core/shell structure [25].

Block copolymers are widely utilized for the synthesis of metal NPs [19, 26–29]. In selective solvents, amphiphilic diblock copolymers are known to form colloid-size aggregates or micelles, within which NPs can be synthetized. The size and geometry of the micelles can be controlled through variation of the copolymer composition and block length. A prerequisite for the successful synthesis of metal NPs is that the metal salt should be insoluble in the solvent, and enter into interaction (usually of coordination type) with the polymer block forming the micelle core. NP size can be controlled through selection of the block copolymer used, the strength of the reducing agent, and the concentration of the precursor. Antonietti et al. [27] reported, that for the slowly reacting triethylsilane (TES), a single NP is usually formed in each micelle, whereas rapid reduction (with $NaBH_4$, superhydrides) leads to the formation of many small NPs per micelle; the former situation was termed cherry morphology and the latter raspberry morphology. Spatz et al. [28] stated that slow reduction allows the exchange of polymers during the collision of micelles, leading to an uneven distribution of the NP.

In this study, Au NPs in poly(styrene)-*block*-poly(2-vinylpyridine) (PS-*b*-P2VP) copolymer micelles were investigated by UV–Vis spectroscopy, transmission electron microscopy (TEM), and DLS measurements. In addition, microcalorimetry was used to investigate NP formation in the copolymer micelles. Thermodynamic studies of NP formation in reverse copolymer micelles do not appear to have been reported previously.

Experimental section

Materials

PS(350)-*b*-P2VP(50) block copolymer (the numbers in the parentheses indicate the block lengths) were synthetized by anionic polymerization according to Ref. [29]. The block copolymer was stirred in dry toluene (99.94%, Molar Chemicals Ltd., Hungary) to prepare the micellar solution. The precursor tetrachloroauric acid ($HAuCl_4 \cdot 3H_2O$) was obtained from Aldrich. The reducing agents used were: potassium triethylborohydride (PTB) [$KB(C_2H_5)_3H$, Aldrich, 1 M in tetrahydrofuran, THF], hydrazine (HA) (N_2H_4, Aldrich, 1 M in THF) and triethylsilane (TES) [$(C_2H_5)_3SiH$, Fluka, ≥97%].

Silicon wafers (CrysTec) were cut into pieces (1 cm × 1 cm) and cleaned in an ultrasonic bath with acetone (Reanal, a.r.), distilled water, and 2-propanol (Reanal, a.r.). After the cleaning procedure, the substrates were dried in a nitrogen flow.

Preparation of gold particle-loaded copolymer micellar systems

The stock solution of the block copolymer micelles loaded with tetrachloroauric acid (gold ion-loaded micellar

solution: GILMS) was prepared as described previously [19]. A 0.5 wt% solution of PS(350)-*b*-P2VP(50) block copolymer in dry toluene (unloaded micellar solution: ULMS) was mixed with 0.5 equiv of $HAuCl_4 \cdot 3H_2O$ per pyridine unit. The mixture was stirred for at least 24 h to allow complete solubilization of the acid in the cores of the block copolymer micelles. Though gold compounds are not soluble in toluene, their solubilization in block copolymer solutions proceeds reasonably quickly (during several hours) due to coordination with the pyridine units.

This transparent yellow solution was diluted with a 5-fold volume of toluene and reduced with HA, PTB, or TES. The reductants were dissolved in THF and used in a 30-fold excess with respect to the Au(III). The experiments were performed under intensive stirring.

Methods

UV–vis spectrophotometry

The formation of Au NPs was followed with an Ocean Optics Chem2000-UV-VIS diode array spectrophotometer at wavelengths in the range 400–800 nm. The absorbance spectrum was recorded every 2 s for 60 min, starting at the moment of the addition of the reducing agent. During the reduction, the reaction mixture was stirred with a micro-magnetic stirrer.

Atomic force microscopy

The AFM images were recorded by Nanoscope III (Digital Instruments, USA). A previously cleaned silicon wafer measuring 1 cm × 1 cm was dipped into the micellar solution containing the gold precursor (GILMS) and after 10 s, raised out of the solution at a constant rate of 10 mm min^{-1}. The film was left to dry in air at room temperature and studied. The tapping mode images were scanned with an etched silicon tip (RTSP tips from Veeco Gmbh).

Isothermal titration microcalorimetry

The experiments were performed at 25 °C, with a thermal activity monitor (TAM) isothermal heat-flow microcalorimeter (Thermometric LKB 2277, Lund, Sweden). For the measurements, 2 mL of GILMS was initially added to a 4-mL stainless steel cell and stirred at 60 rpm. The reducing agent was placed in a 500 μL Hamilton syringe, and aliquots (50 μL) were injected into the cell, controlled by a 612 Lund Syringe Pump. The interval between two injections was long enough for the signal to return to the baseline. The heat of each injection was calculated by the Thermometric Digitam 3 software program. In an effort to discriminate the enthalpy of formation of Au NPs from other heat effects, control experiments were performed simultaneously. In this case, the titration was carried out as described above, except that the cell did not contain Au(III). The concentrations of HA, TES, and PTB were 0.3, 0.6, and 0.04 mM, respectively.

Dynamic light scattering

In order to determine the micelle size and size distribution, DLS measurements were carried out at 25 °C at a fixed angle of 173°, by using a Zetasizer Nano ZS (Malvern Instruments) equipped with a He–Ne laser (wavelength 633 nm) and a digital autocorrelator. Solutions were filtered through nylon filters with a pore size of 0.4 μm (Milex-GN). The particle mean diameter and the polydispersity index (PDI) were obtained by cumulants analysis of DLS correlation function using the DTS V. 5.02 software.

Transmission electron microscopy

Transmission electron micrographs were recorded in a Philips CM-10 transmission electron microscope equipped with a Megaview II digital camera at accelerating voltage of 100 kV. TEM grids were prepared by placing one drop of undiluted sol on a Formwar foil-covered copper grid. The excess sol was removed with filter paper and the sample was then allowed to dry in the air. The size distribution of the NPs was determined by using the UTHSCSA Image Tool 2.00 software.

Results and discussion

Spatz et al. [29] have shown that diblock copolymer micelles may form hexagonal structures on supports with smooth surfaces. Figure 1 presents an AFM image of PS-*b*-P2VP micelles assembled on a silicon surface. The image confirms that a monomicellar layer was formed on the surface of the support, and some of the micelles appear to be arranged in a quasi-hexagonal pattern. The height profile was determined along the horizontal line crossing several micelles, seen in panel b. Cross-sectional analysis indicated a micelle diameter of 20–30 nm.

The reduction of Au(III) and the formation of NPs can be conveniently monitored by UV–Vis spectroscopy. The spectra continuously recorded during the reaction are presented in Fig. 2a–c. The originally yellow GILMS at once turned dark-red on the addition of HA, indicating that nucleation commenced immediately. This is clearly visible in the spectrum series in Fig. 2a. The absorption maximum characteristic of the surface plasmon resonance of Au NPs appeared at 552 nm, and its intensity increased

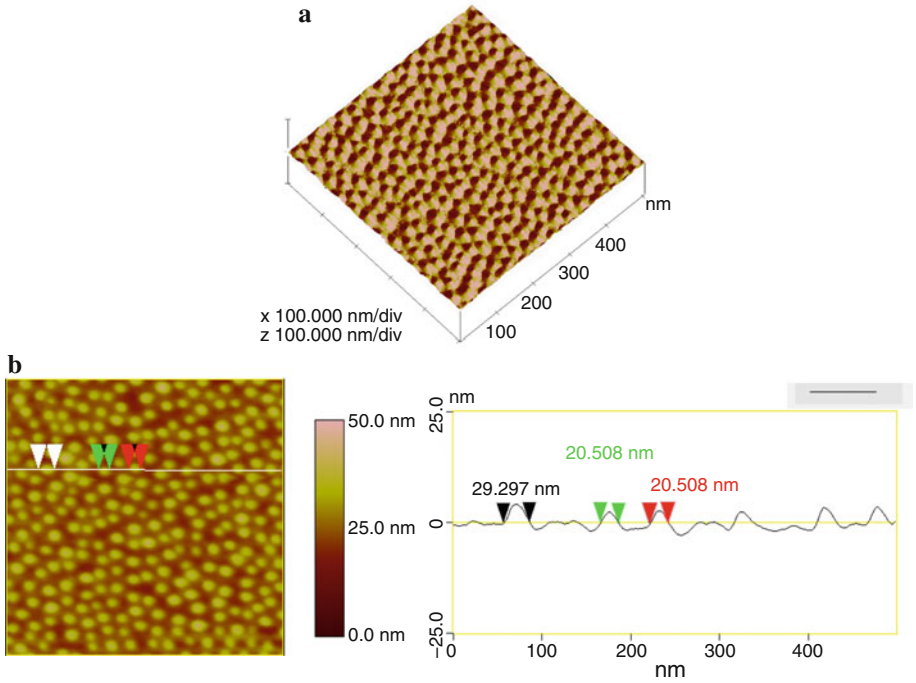

Fig. 1 **a** AFM image (1 μm × 1 μm) and **b** the cross-sectional analysis of a monomicellar film cast from GILMS onto a P-doped Si wafer

continuously. Figure 2d illustrates the changes in absorbance read at λ_{max}. The initially rapid reaction decelerated continuously, but hardly changed after 60 s. Reduction with TES exhibited different kinetics. The absorption peak characteristic of the NPs (at 530 nm) appeared only ~1 min after the addition of the reducing agent. The optical density first increased slowly, then at 120 s started to rise sharply, and finally slowed down continuously until the reaction stopped. The sigmoid curve is shown in Fig. 2d. The spectra recorded during the reaction driven by PTB are shown in Fig. 2c. The resulting sol was brownish-red. The characteristic absorption peak of the Au NPs was at 488 nm, pointing to a smaller NP size than the one after reduction with HA (this was supported by TEM measurements).

The size of the Au NPs formed was determined on the basis of TEM images. Samples were withdrawn from the sols under preparation after 0.5, 1.5, and 60 min following the addition of the reducing agent. Reduction with HA yielded Au NPs with an average diameter of 8 nm (Fig. 3a, b). Most often there was one NP per micelle, but empty micelles also appeared in the image. There was no significant change in the size and arrangement of the NPs at 60 min. This may be due to a change in size as the samples dried. It was reported earlier [19] that, on reduction with anhydrous HA dissolved in toluene, the micelles undergo coagulation in time, and the NPs thereby join together. Images of Au sol generated by reduction with TES are presented in Fig. 3c and d; this yielded smaller NPs ($\bar{d}_{TEM} = 2.6$ nm). Each micelle contained one or two NPs, but empty micelles were also seen on TEM. An hour after the addition of the reducing agent, the number of NPs had increased several-fold. This accords with UV–Vis results, which revealed that reduction with TES accelerates after an induction period. The average NP size increased from 2.2 nm to only 2.6 nm in 1 h. The TEM images in Fig. 3e and f demonstrate the effect of reduction with PTB. The original micellar structure underwent a significant rearrangement. Figure 3e depicts the state of the sample at 30 s after the injection of PTB; the original micelles have been replaced by large droplets, and NPs are floating free in the reaction medium, or located on the interfaces of the droplets. The state observed 60 min later is shown in Fig. 3f: the structure of the sol is altered; many smaller droplets/micelles are to be seen. This was confirmed by the DLS measurements. The majority of the NPs were situated within the smaller droplets/micelles, or are attached to the edges of the larger droplets/vesicles. The smallest NPs were formed on reduction with PTB: the average size changed from 1.1 to 1.7 nm in 1 h.

Light scattering techniques have the advantage of allowing in situ study of the structural transition of micelles on loading with $HAuCl_4$ and during the reduction process, to supplement the spectroscopic and electron microscopic data. Figure 4a presents the intensity distribution for the micellar systems. The mean hydrodynamic diameter of the empty PS-*b*-P2VP micelles in toluene was 12 nm (PDI = 0.197). The size of the micelles increased to 54 nm (PDI = 0.302) following the incorporation of $HAuCl_4$. Other authors have reported a decrease in micelle size following the addition of $HAuCl_4$ which they explained by the development of a more compact micellar structure [21]. On reduction with HA, the micelle size increased to 64 nm

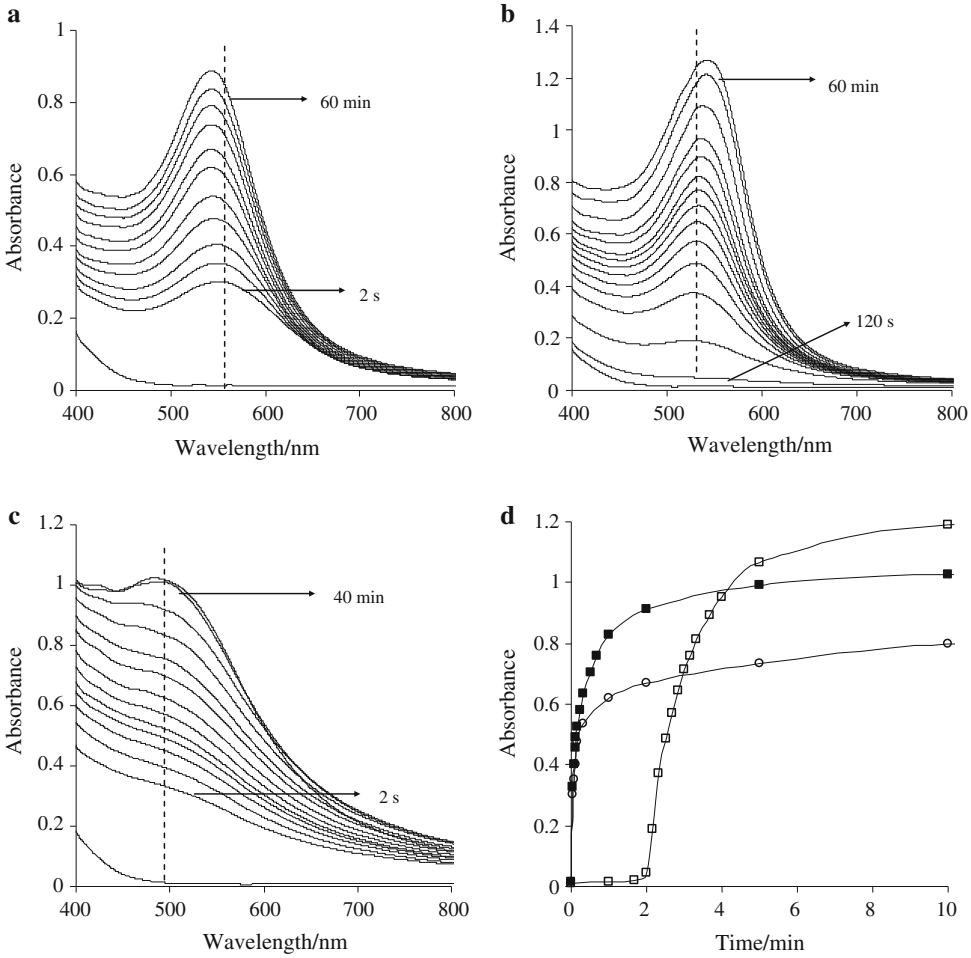

Fig. 2 The evolution of UV–Vis absorption spectra of Au NPs during reduction with **a** HA, **b** TES, **c** PTB, and **d** the evolution of the absorption at λ_{max} determined from spectra during reduction process with HA (*open circle*), TES (*open square*), and PTB (*filled square*)

(PDI = 0.215). This can be explained by the swelling of the micelles as a consequence of the incorporation of the HA/THF solution into the polar core of the micelles. Reduction with TES led to a slightly increased micelle size. The micellar structure was retained following the reduction with either HA or TES. Reduction with PTB resulted in the development of a complex colloid system. Rearrangement of the original structure was indicated by the TEM images. In the course of the disintegration, joining, and swelling of micelles, large droplets of various sizes were formed. After the addition of PTB, the average diameter $\bar{d}_{DLS}$ was 1,100 nm (PDI = 0.852), which steadily decreased to 105 nm (PDI = 0.270) at 24 h (Fig. 4b). After some time, the large droplets presumably fall apart, their material arranging itself around the Au NPs formed and enclosing them in smaller micelles. Since the reducing agents were dissolved in THF before their addition to the polymer solution, we studied the effects of THF on the micelle size. Immediately after mixing, at $\Phi_{THF} = 0.01$ (corresponding to the volume fraction of THF added together with the reducing agent), $\bar{d}_{DLS}$ was 275 nm (PDI = 0.143) which decreased to 29 nm (PDI = 0.390) at 60 min.

Microcalorimetry is known to be a sensitive technique with which to demonstrate the formation and possible growth of NPs [21–24]. The heat of formation of Au NPs was earlier determined by Liveri and co-workers [22] by reducing $HAuCl_4$ with hydrazine sulphate in a water/AOT/*n*-heptane microemulsion.

Figure 5a–c illustrates the heat changes accompanying NP formation. The enthalpy changes caused by the addition of the three different reducing agents differed appreciably. It is important to note that the thermal processes taking place within the calorimeter jointly produce the values of ΔH determined experimentally; the individual processes cannot be separated on the basis of the enthalpogram, and the individual partial processes must therefore be measured in separate experiments. Reference measurements were also performed in the absence of Au(III) (Fig. 5a–c).

The enthalpograms of reduction with HA and the reference reaction are shown in Fig. 5a. Addition of HA to GILMS resulted in heat release relating to reduction only in the first three titration steps and then remains constant. The reduction of Au(III) was, therefore, completed by the addition of 3 × 50 μL of reducing agent ([HA]/[Au] = 20.25).

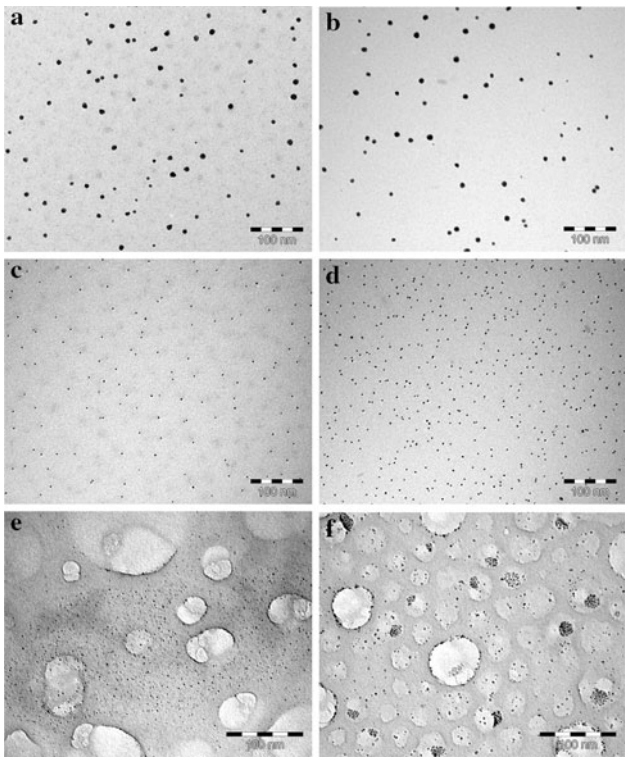

Fig. 3 TEM images of Au nanoparticles in PS-*b*-P2VP micelles reduced with HA: **a** $t_{red} = 30$ s, $\bar{d}_{TEM} = 8.2$ nm and **b** $t_{red} = 60$ min, $\bar{d}_{TEM} = 9$ nm; TES: **c** $t_{red} = 90$ s, $\bar{d}_{TEM} = 2.2$ nm, and **d** $t_{red} = 60$ min, $\bar{d}_{TEM} = 2.6$ nm; and PTB: **e** $t_{red} = 30$ s, $\bar{d}_{TEM} = 1.1$ nm, and **f** $t_{red} = 60$ min, $\bar{d}_{TEM} = 1.7$ nm

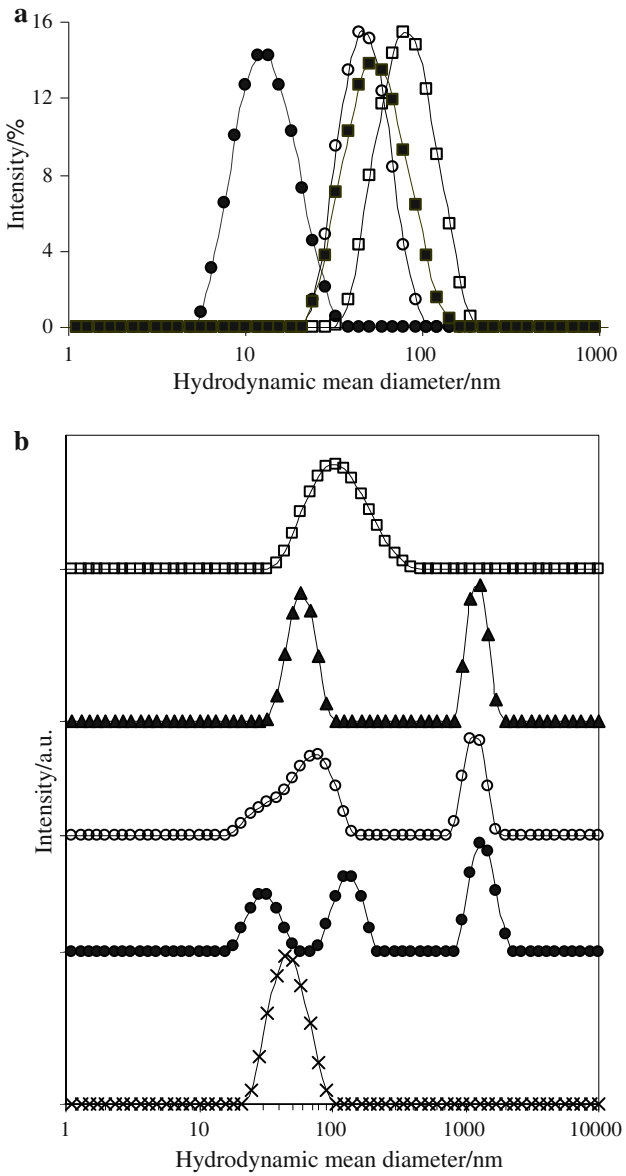

Fig. 4 **a** Hydrodynamic diameter distribution of PS-b-P2VP micelles: ULMS (*filled circle*), GILMS (*open circle*), GILMS (*open square*) reduced with HA and TES (*filled square*). **b** The effect of the reduction with PTB on hydrodynamic diameter distribution for GILMS: GILMS (*multi symbol*), directly (*filled circle*), 10 min (*open circle*), 30 min (*open square*), and 24 h (*filled triangle*) after the addition of PTB

The heat quantities measured in the subsequent titration steps were equal to those observed on mixing of the polymer dissolved in toluene with THF (not shown). The sharp peak indicating reduction in the enthalpogram was followed by a distinct shoulder; this slow exothermic process which took $\sim$3 h to be completed was identified as the aggregation of Au NPs.

When TES was added to GILMS, an initial endothermic effect was observed (Fig. 5b). The same endothermic reaction was observed in the reference measurements without Au(III), and, consequently, it is not associated with NP formation. The endothermic process occurs presumably due to the demicellization of diblock copolymer micelles through the incorporation of TES. After reduction process, diblock copolymer molecules rearranged similar to an adsorption protecting layer around Au NPs. This endothermic reaction delays the formation of Au particles and is responsible for the induction period identified by UV–Vis spectroscopy. An exothermic process also occured in parallel with the endothermic process. When the micelles also contained Au(III), an intensive exothermic effect accompanied its reduction. In the first titration step, the combined heat produced by the exothermic processes was $\Delta H_r = -201$ kJ (mol TES)$^{-1}$. The heat release was slower than in the case of reduction with HA or PTB: there were two steps in the ascending branch of the peak. Reduction was accompanied by another exothermic process taking $\sim$6 h), which appeared in the enthalpogram in each titration step. Thus, a chemical reaction was brought about by the addition of each new 50 μL dose of TES to the cell, in spite of the fact that all Au(III) present was already reduced by the first 50 μL of TES ([TES]/[Au] = 6.8).

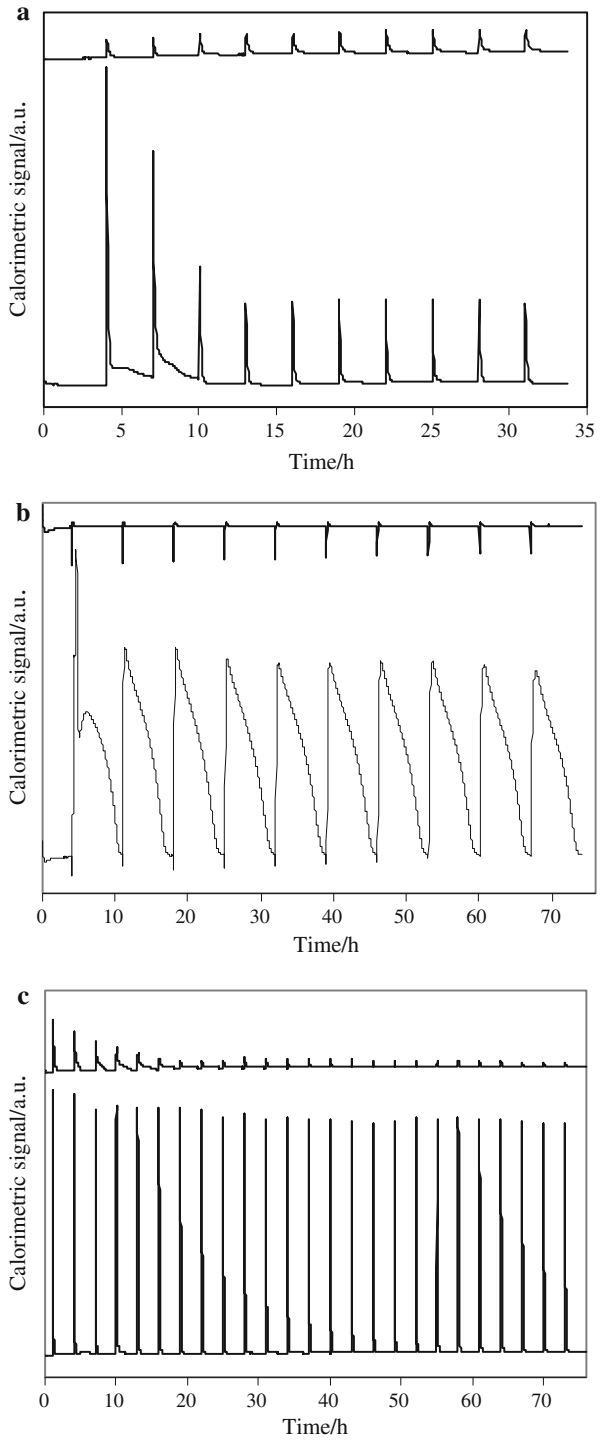

Fig. 5 The enthalpogram of the thermometric titration of ULMS (*upper line*) and GILMS (*lower line*) with **a** HA, **b** TES, and **c** PTB

The enthalpograms of reduction with PTB and of the reference process are shown in Fig. 5c. The addition of PTB to ULMS elicited heat release; the amount of heat generated decreased continuously, and then remained nearly constant until the end of the titration. This exothermic process is probably a chemical reaction between the polymer and PTB, since PTB is capable of reducing the pyridine group of the polymer to piperidine [30]. The enthalpy of this reaction was determined to be $\Delta H_r = -72$ kJ (mol PTB)$^{-1}$.

The calculated enthalpy changes for the reaction of PTB with GILMS were equal for each titration step [$\Delta H_r = -146$ kJ (mol PTB)$^{-1}$]. This heat release was continuous with each addition and did not decrease in spite of all the Au(III) having already been reduced in the first titration step ([PTB]/[Au] = 1.4). This suggests that an additional chemical reaction dependent on the presence of Au NPs may take place. These chemical reactions accompanied by the release of large amounts of heat may be responsible for the rearrangement of the original micellar structure indicated by the light scattering measurements and TEM images.

The calorimetric measurements clearly demonstrated that chemical reactions take place in the course of reduction with TES and PTB, which cannot be distinguished calorimetrically from the formation of the Au NPs by reference measurements. It is possible to calculate the enthalpies of formation of Au NPs in the case of reduction with HA. Thus, the change in enthalpy of particle formation can be calculated by means of the expression: $\Delta H_f = \Delta H_{tot} - \Delta H_{mix}$, where ΔH_{tot} is the total enthalpy change measured in the reduction process and ΔH_{mix} is the enthalpy of mixing measured in the reference experiment. When the data are normalized to the amount of Au(III) present in the solution, the molar enthalpy of the reduction of Au(III) is obtained. Plots of the molar enthalpy plotted against the molar ratio of HA and Au(III) are shown in Fig. 6. The heat of formation of Au NPs in the case of reduction with HA is $\Delta H_f = -195$ kJ mol^{-1}.

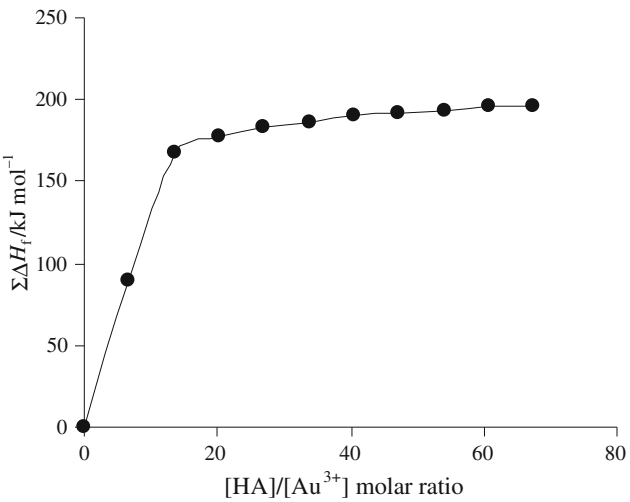

Fig. 6 Plots of the molar enthalpy of formation of Au NPs against the molar ratio of HA and Au(III)

Conclusions

This complex study of the formation of Au NPs in micelles of PS-*b*-P2VP copolymer by UV–Vis spectroscopy, TEM, DLS, and ITC yielded a fairly detailed insight into Au NPs formation. The effects of the reducing agents HA, TES, and PTB were compared in the experiments. The gold sols produced were stable for up to several months in all the cases. The rates of reduction with HA and PTB were nearly identical. The use of HA led to the formation of larger NPs ($\bar{d}_{\mathrm{TEM}} = 8$ nm) and that of PTB to smaller NPs ($\bar{d}_{\mathrm{TEM}} = 1.7$ nm). In the course of reduction with PTB, a large exothermic effect was observed. During this process, the original micellar structure underwent rearrangement. With TES as reducing agent, an endothermic reaction was detected at the beginning of the process, which resulted in an induction period of NP growth. Calorimetric measurements revealed that chemical reactions other than the reduction of Au(III) and the aggregation of the Au NPs also take place. The heat of formation of Au NPs could be determined only for reduction with HA: $\Delta H_{\mathrm{f}} = -195$ kJ mol^{-1}.

Acknowledgements The authors are very grateful for the financial support of the MÖB-DAAD project no. 14.

References

1. Daniel MC, Astruc D. Gold nanoparticles: assembly, supramolecular chemistry, quantum-size-related properties, and applications toward biology, catalysis, and nanotechnology. Chem Rev. 2004;104:293–346.
2. Haruta M. Gold as a novel catalyst in the 21st century: preparation, working mechanism and applications. Gold Bull. 2004;37:27–36.
3. El-Sayed IH, Huang XH, El-Sayed MA. Surface plasmon resonance scattering and absorption of anti-EGFR antibody conjugated gold nanoparticles in cancer diagnostics: applications in oral cancer. Nano Lett. 2005;5:829–34.
4. Turkevich J, Stevenson PC, Hillier J. A study of the nucleation and growth of processes in the synthesis of colloidal gold. Discuss Trans Faraday Soc. 1951;11:55–75.
5. Brust M, Walker M, Bethell D, Schiffrin DJ, Whyman R. Synthesis of thiol derivatised gold nanoparticles in a two phase liquid/liquid system. J Chem Soc Chem Commun. 1994;7:801–2.
6. Teranishi T, Kiyokawa I, Miyake M. Synthesis of monodisperse gold nanoparticles using linear polymers as protective agents. Adv Mater. 1998;10:596–9.
7. Esumi K, Hara J, Aihara N, Usui K, Torigoe K. Preparation of anisotropic gold particles using a gemini surfactant template. J Colloid Interface Sci. 1998;208:578–81.
8. Ji X, Song X, Li J, Bai Y, Yang W, Peng X. Size control of gold nanocrystals in citrate reduction: the third role of citrate. J Am Chem Soc. 2007;129:13939–48.
9. Henglein A. Radiolytic preparation of ultrafine colloidal gold particles in aqueous solution: optical spectrum, controlled growth, and some chemical reactions. Langmuir. 1999;15:6738–44.
10. Jana NR, Gearheart L, Murphy CJ. Evidence for seed-mediated nucleation in the formation of gold nanoparticles from gold salts. Chem Mater. 2001;13:2313–22.
11. Bakrania SD, Rathore GK, Wooldridge MS. An investigation of the thermal decomposition of gold acetate. J Therm Anal Calorim. 2009;95:117–22.
12. Privman V, Goia DV, Park J, Matijević E. Mechanism of formation of monodispersed colloids by aggregation of nanosize precursors. J Colloid Interface Sci. 1999;213:36–45.
13. Alvarez MM, Khoury JT, Schaaff TG, Shafigullin MN, Vezmar I, Whetten RL. Optical absorption spectra of nanocrystal gold molecules. J Phys Chem B. 1997;101:3706–12.
14. Mie G. Beitrage zur Optik Truber Medien, Speziell Kolloidaler Metallosungen. Ann Phys. 1908;25:377–445.
15. Sato S, Toda K, Oniki S. Kinetic study on the formation of colloidal gold in the presence of acetylenic glycol nonionic surfactant. J Colloid Interface Sci. 1999;218:504–10.
16. Yang S, Wang Y, Wang Q, Zhang R, Ding B. UV irradiation induced formation of Au nanoparticles at room temperature: the case of pH values. Colloids Surf A. 2007;301:174–83.
17. Patakfalvi R, Papp S, Dékány I. The kinetics of homogeneous nucleation of silver nanoparticles stabilized by polymers. J Nanopart Res. 2007;9:353–64.
18. Papp S, Dekany I. Nucleation and growth of palladium nanoparticles stabilized by polymers and layer silicates. Colloid Polym Sci. 2006;284:1049–56.
19. Mössmer S, Spatz JP, Möller M, Aberle T, Schmidt J, Burchard W. Solution behavior of poly(styrene)-block-poly(2-vinylpyridine) micelles containing gold nanoparticles. Macromolecules. 2000;33:4791–8.
20. Sidorov SN, Bronstein LM, Kabachii YA, Valetsky PM, Lim Soo P, Maysinger D, et al. Influence of metalation on the morphologies of poly(ethylene oxide)-block-poly(4-vinylpyridine) block copolymer micelles. Langmuir. 2004;20:3543–50.
21. Meristoudi A, Pispas S, Vainosi N. Self-assembly in solutions of block and random copolymers during metal nanoparticle formation. J Polym Sci B. 2008;46:1515–24.
22. Arcoleo V, Cavallaro G, Manna GL, Liveri VT. Calorimetric investigation on the formation of palladium nanoparticles in water/AOT/n-heptane microemulsions. Thermochim Acta. 1995;254:111–9.
23. Aliotta F, Arcoleo V, Buccoleri S, La Manna G, Liveri VT. Calorimetric investigation on the formation of gold nanoparticles in water/AOT/n-heptane microemulsions. Thermochim Acta. 1995;265:15–23.
24. Patakfalvi R, Dékány I. Nucleation and growing of silver nanoparticles under control of titration microcalorimetric experiment. J Therm Anal Calorim. 2005;79:587–94.
25. Kanemaru M, Shiraishi Y, Koga Y, Toshima N. Calorimetric study on self-assembling of two kinds of monometallic nanoparticles in solution. J Therm Anal Calorim. 2005;81:523–7.
26. Seregina MV, Bronstein LM, Platonova OA, Chernyshov DM, Valetsky PM, Hartmann J, et al. Preparation of noble-metal colloids in block copolymer micelles and their catalytic properties in hydrogenation. Chem Mater. 1997;9:923–31.
27. Antonietti M, Wenz E, Bronstein L, Seregina M. Synthesis and characterization of noble metal colloids in block copolymer micelles. Adv Mater. 1995;7:1000–5.
28. Spatz JP, Sheiko S, Moller M. Ion-stabilized block copolymer micelles: film formation and intermicellar interaction. Macromolecules. 1996;29:3220–6.
29. Saptz JP, Mössmer S, Hartmann C, Möller M, Herzog T, Krieger M, et al. Ordered deposition of inorganic clusters from micellar block copolymer films. Langmuir. 2000;16:407–15.
30. Yoon NM, Yang HS, Hwang YS. Reducing characteristics of potassium triethylborohydride. Bull Korean Chem Soc. 1987;8:85–91.